History of Medicine Studies

ISSN:1300-669
Volume 16 Issue 2 July 2020

Functional Optofluidic Elements Direct Laser Written in Porous Silicate Matrix

Roman A. Zakoildaev*[1], Zhoing Lijing[2], Veronikai A. Yakimuki[1],

[1]*ITMO University, 49, Kronverkskiy av., 197101, St. Petersburg, Russia*
[2]*Zhejiang Lab, Hangzhou City, Zhejiang Province, 311121, P.R. China*
[*]*Corresponding author's e-mail: zakoldaev@gmail.com*

For sensoric and analytical operations carried out on a single chip, the integration of optical, micro-, and nanofluid structures in glass has long been pertinent. Direct laser writing (DLW) expedites the integration process by supplying the necessary functional parts with exceptional structural characteristics and high accuracy. Here, we take into account a porous silicate matrix (PSM) as a foundation for the growth of the optofluidic components' kind. We propose optical waveguides, barriers, and micro-sized hollow channels as three different sorts of components. By adjusting the laser processing settings, the density of the PSM is changed to create all of these components. The creation and examination of symmetrical optical waveguides, writing pass-through barrier optimization, and microchannel manufacturing are all novel experimental studies revealed by the work.

.

Keywords: porous silicate matrix, DLW, optofluidic, waveguides, microfluidic channel, barriers

1. Introduction

Direct laser writing (DLW) in glass is gaining popularity to integrate functional elements such as waveguides [1], hollow channels [2], and microcavity [3] inside a glass substrate. This trend is also justified by the development of integrated optics, sensorics, and chip-scale devices. Solid and single-component glass, such as fused silica, is a classical base for opto-fluid [4] and micromechanical systems [5]. On the other hand, the initial density of glass restricts the thresholds for laser processing, limiting the variation in the properties of optofluidic elements.

Porous silicate matrices (PSM) can significantly expand the functionality of the elements and offer a novel architecture. Noteworthy, PSM is also produced in the form of optical blanks with the required size and thickness. Previous studies on laser-induced modifications of porous glass [6], sol-gel, and aerogel [7] have confirmed the possibility to vary the material density. That opened the way for DLW of waveguides [8], integral gas-analytical cells [9], microfluidics [10], and nanofluidic [11] channels. The laser-induced change is expressed as nanopore closure, nanogratting formation, or material foaming. The difference in the composition of the original glass blanks significantly complicates the obtaining of stable and identical results. Therefore, we have initiated a research project to develop methods for the femtosecond DLW in PSM produced from one glass melting batch.

Herein, we present the results of recording three elements in PSM by changing focusing conditions and laser processing parameters. Among these elements are (i) waveguides with almost symmetrical shape with the refractive index contrast $1.54 \cdot 10^{-3}$; (ii) the barriers isolating the PSM plate; (iii) micro-channels in PSM without chemical etching and sintering. Remarkably, all the investigations were accomplished inside PSM with through pores and large free pore volume (~ 50%) promising great opportunities for modifying the sample structure under the action of laser radiation.

2. Experiment and Methods

The samples are produced from two-phase glass providing stable and reproducible characteristics. In particular, our PSM-17 possesses thickness 1.0±0.1 mm, pore size ~ 17 nm, and porosity 50-54% [12]. The sample consists of >90% SiO_2 including an insignificant amount of impurities in the form of B_2O_3, Na_2O. The photos and spectral characterization show high uniformity and optical transparency higher than 80% in the range of 600-1100 nm (Fig. 1).

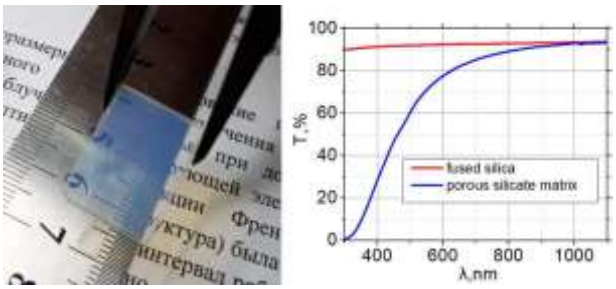

Fig.1. Photo of PSM-17 sample with a size of 15x20x1 mm and transmission spectrum in the range 200-1100 nm with the reference to fused silica.

Laser writing was performed on an experimental setup (Fig. 2) with an ytterbium fiber femtosecond laser (ANTAUS-20W-20u/1M, Avesta Ltd., Moscow, Russia) as a radiation source. The laser generates pulses with duration 0.22 - 3.0 ps and frequency up to 1 MHz. At the output of

History of Medicine Studies
ISSN:1300-669
Volume 16 Issue 2 July 2020

the system, the average power is P_0 = 20 W for wavelength 1030 nm. Table 1 presents the information about the lenses applied. The choice of a lens is discussed in the following section. The sample was fixed and translated on a programmable coordinate system with minimum step 500 nm and maximum speed up to 100 mm/s.

Table 1 - List of applied objectives

Title	Task
60X, NA=0.85	waveguides
20X, NA=0.4	channels
Plano convex lens, F = 200 mm	barriers

Microphoto images of the final structures were captured by a microscope (Axio Imager A1m, Carl Zeiss). The sample ends were ground and polished by a polishing unit (Buehler MetaServ 250). Laser radiation coupling by the objective (60X, NA=0.85) - objective (20X, NA=0.4) connection was organized to test the fabricated waveguides and capture near-field intensity distribution.

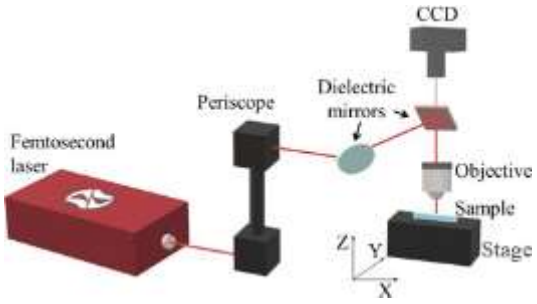

Fig.2. Schematic illustration of the experimental setup for DLW in PSM.

3. Results and discussion

This study demonstrates the fabrication of the waveguides, impermeable barriers, and microchannels in the PSM plate. In the following subsections, we focus on each element separately.

3.1 Waveguides writing

Waveguides are fabricated with sharp focusing of laser radiation using the objective with 60X magnification (Table 1). The formation of elongated regions with a large aspect ratio is a known obstacle in the field of waveguide writing. An elementary solution is the use of the slit technique, which is described in detail in [13]. Briefly, the slit beam shaping technique operates by placing the slit directly in front of the objective. The slit size can be calculated by the following equation:

$$\frac{W_y}{W_x} = \frac{NA}{n}\sqrt{\frac{tn2}{3}}, if\ W_x > 3W_y, (1)$$

where W_y and W_x are the slit width, $NA \sim f/W_x$ where f is the focal length of the objective, and n is the refractive index of PSM. This technique has never been used for DLW of waveguides in PSM before.

Figures 3a and 3b demonstrate the top view and cross-sectional micro photos of the fabricated waveguides buried at 250 μm inside the sample. When a slit (~ 1.0 mm) was utilized, the average longitudinal and transverse sizes were 3.0 μm and 2.8 μm, respectively. The aspect ratio of the manufactured waveguides is 1.07. We also determined the minimum period (p) for waveguides arrangement. When we fabricated closed packed waveguides with period of displacement p < 5 um, we noticed the reshaping of the previously fabricated waveguide. As a result, the aspect ratio is changed (Fig. 3, b, set with p = 3). If we increase p > 5, the fabrication process does not influence the previously fabricated waveguide. Such a small period resulted in no defects across the waveguides, which is one more benefit of the technique applied.

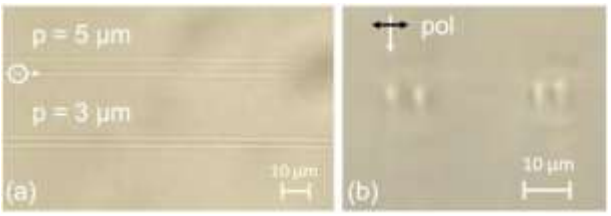

Fig.3. Micro photos of waveguides buried at 250 μm inside PSM: (a) top view and (b) cross-section. Writing parameters: P_0 = 2 W, scanning speed 45 mm/s. The laser beam direction is indicated by the white arrow. The radiation polarization is indicated by black arrow.

The cross-sectional photo shows a bright almost circular spot resulting from the increment in the refractive index. On the left (Fig. 3, b), under the bright spot, there is a subtle dark area that accompanies all the created waveguides. The appearance of the dark region is the result of light scattering that occurs on the decompressed zone of the waveguide. Optical microscopy does not allow to see in detail such a decompressed region. The refractive index contrast (Δn) in this cross-section differs compared to the initial material and the waveguide core. For this, the near field distribution of the He-Ne laser radiation was captured (Fig. 4, a). The observed modes have a good degree of symmetry and beam diameter ~ 4 μm. The data obtained also allows to evaluate the refractive index contrast by the method applied earlier [14]. The calculations made it possible to estimate the contrast, $\Delta n = 1.54 \cdot 10^{-3}$ (Fig. 4, b).

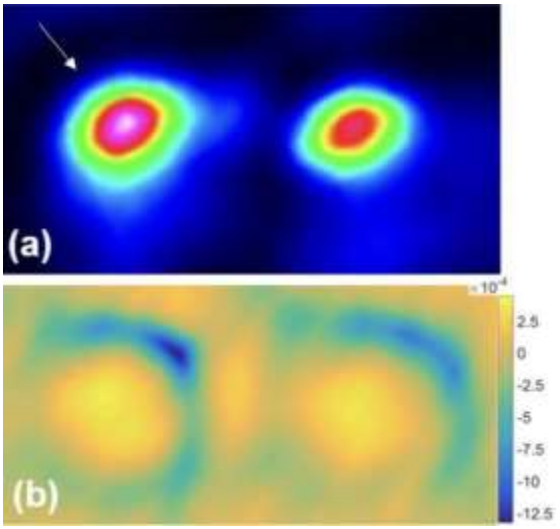

Fig.4. The near field image of guided modes at 635 nm for two waveguides located with p = 9 μm (a). Estimated refractive index contrast profile (b).

The He-Ne laser beam was coupled into the left waveguide (indicated by an arrow in Fig. 4, a) through an

History of Medicine Studies
ISSN:1300-669
Volume 16 Issue 2 July 2020

objective (60X, 0.85 NA), and its output beam was collected by another objective (40X, 0.65 NA). At the output side of the dual-waveguides, effective light coupling into the right waveguide was observed, the intensity ratio between the left and the right waveguide is ~5:4. This phenomenon is attributed to the crosstalk between the dual waveguides due to the overlap of their cladding or evanescent wave field [15].

3.2 Impenetrable barriers

The initial PSM has a nanoporous framework, which we modify by DLW. Thus, the fabricated uniform tracks can collapse the nanopores locally to control their throughput and hence the flow of nanoobjects trapped by pores. We called these tracks barriers aimed at holding the flow of nanoobjects inside the glass. Previously, we demonstrated the isolation of several independent zones in a single PSM for sensing purposes [16]. However, every barrier consisted of several densified tracks providing full-thickness filling of the glass plate. This time, we optimized the procedure to fabricate the barrier by a single scan. The radiation is now focused by the lens (Table 1) with a long focal length and a larger Rayleigh zone compared to the objectives.

First, we optimized the laser power to write homogeneous barriers. At a constant speed (1 mm/s), a set of tracks with different power (1200-1600 mW) was fabricated at a frequency of 200 kHz. The set fragment is shown in figure 5, a. The average width is 5 μm and the irregularities achieved along every track. That is mostly the result of external vibrations. Changing the scanning speed in the range of 0.5 - 20 mm/s made it possible to determine the optimal scanning speed to obtain a uniform barrier for speed > 5 mm/s.

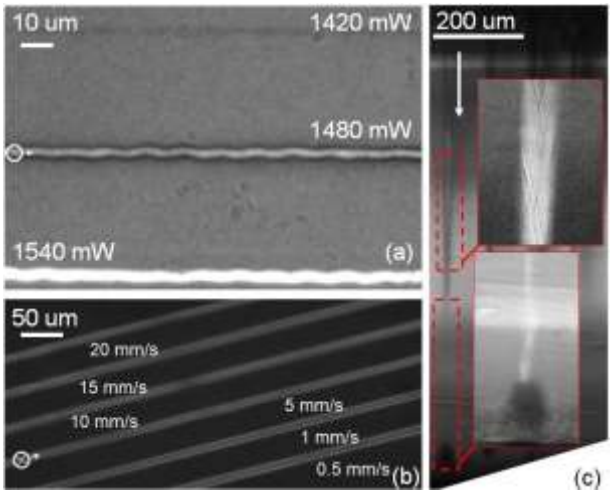

Fig.5. Micro photos of barriers fabricated by DLW in PSM with constant scanning speed (1 mm/s) and different power (1540, 1490 and 1420 mW) (a). The influence of scanning speed (0.5 - 20 mm/s) on the uniform shape of the barrier at constant power (1540 mW) (b). Cross-section of the barrier, which length corresponds to the glass thickness (c). The laser beam direction is indicated by the white arrow.

The barrier depth is an important characteristic, and in our case, the minimum value was 400 μm at the minimum laser radiation power (1200 mW). By increasing the power to 1540 mW at the speed of 10 mm/s, it was possible to fabricate a track with the depth commensurate with the thickness of PSM ~ 1 mm (Fig. 5, c). In cross-section, the barrier does not remain constant in size. As a result of self-focusing [17], we observe its broadening to 20 μm in the upper part, and narrowing to 5 μm from the bottom (Fig. 5, c). On the lower surface of the glass, a local decompaction of the material in the form of a dark sphere is also noticeable.

3.3 Hollow micro-channels

A gradual increase in the power of the laser radiation led to the formation of highly scattering tracks attributed to the local glass destruction. Previously, it was shown micro-chambers and channels fabrication by simultaneous controlled laser-induced destruction of nanoporous materials with subsequent thermal sintering [18]. The centimeter channels with square cross-section were formed beneath the glass surface by a femtosecond laser writing inside a water-immersed sample.

Our current research aims to fabricate channels and save the nanoporous structure without chemical etching. First, the channel prototype was formed by using a lower frequency, 10 Hz, and a higher pulse energy, 100-200 μJ, with pulse duration 30 ps (Fig. 6, a). The uniform brightness of the structure under a crossed polarizer and analyzer indicates the presence of debris across the track (Fig. 6, b). The cross-section of the channel is 53x16 μm (Fig. 6, c).

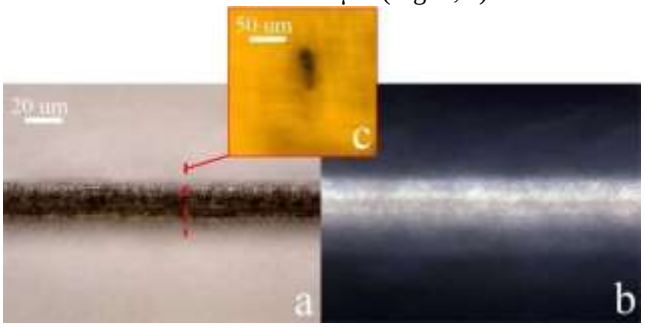

Fig.6. Microphotos of channel prototype fabricated with picosecond laser (335 nm, 30 ps, 200 μJ) in transmitted (a) and cross-polarized light (b) The channel cross-section (c).

The debris was removed by ultrasonic cleaning in water. The action of ultrasound (5 min, temperature 31°C) led to a noticeable clarification of the track (Fig. 7). It can be assumed that the nanoporous framework undergoes the action of ultrasound and promotes the removal of debris. The measurement of the channel cleaning speed was performed after 5 minutes and consisted of measuring the length of the cleaned area when examining the sample with an optical microscope. The presence of uncleaned areas is noticeable in the crossed polarizer and analyzer pair. The data obtained allowed to determine the cleaning speed. The length, 300 μm, of microchannel was cleaned at the maximum speed (60 μm/min), while the subsequent sections passed the cleaning stage at a lower speed, up to 40 μm/min. Thus, the average speed of cleaning a channel with the length of 800 μm equaled ~ 50 μm/min. The decrease in the cleaning speed is due to a slowdown in the inflow of water and the outflow of removal products from the channel.

History of Medicine Studies
ISSN:1300-669
Volume 16 Issue 2 July 2020

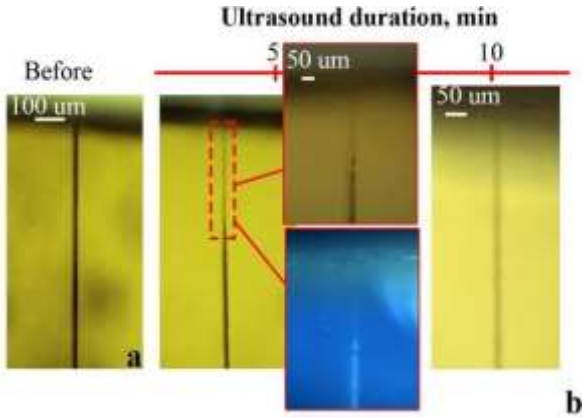

Fig.7. Microphoto of channel prototype before (a) and after ultrasound cleaning in water (b) after 5 and 10 minutes.

Based on the literature review [19], we can assume that longer channels are more complicated to clean. Debris can block the water flow. However, several ways can be used to overcome this obstacle - channel widening and multi-pass writing. More complex way is to create additional channels with output to the surface [4].

At the next step, we decided to increase the speed of through channels writing and applied higher frequency with help of fs-laser setup. Changing the objective from 20X to 60X allowed us to reduce the waist diameter, as well as the channel cross-section (9x23 μm). The frequency, up to 200 kHz, was applied to avoid the consolidation of derbes that was discussed elsewhere [20]. Then, the set of channels prototypes was fabricated with constant laser power, 740 mW, and frequency - 200 kHz (Fig. 8, a). Then, we cleaned channels under the action of ultrasound with the parameters: 150 min, 31 °C (Fig. 8, b).

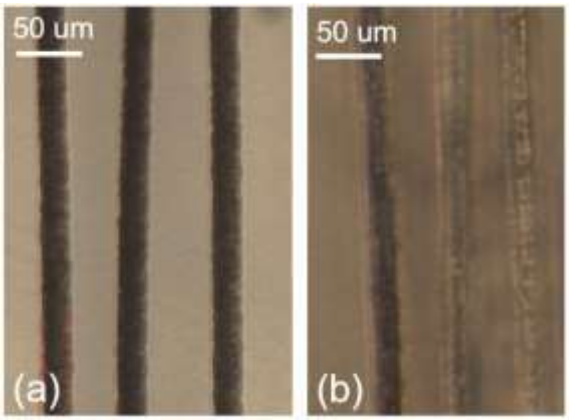

Fig.8. Micro photos of channel prototype set fabricated inside PSM, P_0 = 740 mW, scanning speed 45 mm/s, objective 60X, NA=0,85, ν=200 kHz,: (a) after laser direct writing and (b) after cleaning in the water under ultrasound action.

Conclusion

Applying the direct laser writing technique we have fabricated three optofluidic elements inside PSM. The symmetrical (aspect ratio 1.07) waveguide was fabricated at high scanning speed 45 mm/s. The minimum period of waveguide placement was determined, p≥ 5 μm. If the period is decreased, p = 3 μm, the aspect ratio of the waveguides changes.

We have demonstrated the fabrication of pass-through barriers by a single scan. The use of a long-focus lens made it possible to collapse the nanoporous framework locally over the PSM sample thickness.

Microchannel prototypes were successfully fabricated in the PSM, and then cleaned in water under the action of ultrasound. The nanoporous structure remained preserved as chemical etching and complete sintering of PSM was not applied. The average speed of cleaning a channel with the length of 800 μm equaled ~ 50 μm/min.

Acknowledgments

The study is funded by the grant of Russian Science Foundation (project № 20-71-10103).

References

[1] M. Macias-Montero, F. Muñoz, B. Sotillo, J. del Hoyo, R. Ariza, P. Fernandez, J. Siegel, and J. Solis: Sci. Rep., 11, (2021) 8390.
[2] Xiaolong Li, Jian Xu, Zijie Lin, Jia Qi, Peng Wang, Wei Chu, Zhiwei Fang, Zhenhua Wang, Zhifang Chai, Ya Cheng: Appl. Surf. Sci., 485, (2019) 188.
[3] S.S. Fedotov, A.S. Lipatiev, M.Y. Presniakov, G.Y. Shakhgildyan, A.G. Okhrimchuk, S.V. Lotarev, and V.N. Sigaev: Opt. Lett., 45, (2020) 5424.
[4] Zhengming Liu, Jian Xu, Zijie Lin, Jia Qi, Xiaolong Li, Aodong Zhang, Jintian Lin, Jianfang Chen, Zhiwei Fang, Yunpeng Song, Wei Chu, Ya Cheng: Opt. Laser Technol., 141, (2021) 107118.
[5] V. Stankevic, T. Rakickas, and G. Raciukaitis: J. Laser Micro Nanoeng., 11, (2016) 53.
[6] L. Zhong, R. A. Zakoldaev, M. M. Sergeev, V. P. Veiko, and Z. Li: Opt. Quantum Electron., 49, (2020) 1
[7] A. Cerkauskaite, R. Drevinskas, A.O. Rybaltovskii, and P.G. Kazansky: Opt. Express, 25, (2017) 8011.
[8] J.V. Mikhailova, L. Zhong, A.A. Ostanin, M.M. Sergeev, R.A. Zakoldaev: J. Laser Micro Nanoeng., 15, (2020) 252.
[9] V.P. Veiko, R.A. Zakoldaev, M.M. Sergeev, P.A. Danilov, S.I. Kudryashov, G.K. Kostiuk, A.N. Sivers, A.A. Ionin, T.V. Antropova, and O.S. Medvedev: Opt. Express, 26, (2018) 28150.
[10] K. Liao, W. Wang, X. Mei and B. Liu: Opt. Laser Technol., 142, (2021) 107201.
[11] Yang Liao, Ya Cheng, Changning Liu, Jiangxin Song, Fei He, Yinglong Shen, Danping Chen, Zhizhan Xu, Zhichao Fan, Xunbin Wei, Koji Sugioka, and Katsumi Midorikawa: Lab Chip, 13, (2013) 1626.
[12] O.V. Andreeva, I.E. Obyknovennaya, E.R. Gavrilyuk, A.A. Paramonov, and A.P. Kushnarenko: J. Opt. Technol., 72, (2005) 916.
[13] M. Ams, G.D. Marshall, D.J. Spence, and M.J. Withford: Opt. Express, 13, (2005) 5676.
[14] L. Zhong, R.A. Zakoldaev, M.M. Sergeev, V.P. Veiko, and Z. Li: Opt. Quantum Electron., 52, (2020) 49
[15] A. Szameit and S. Nolte: J. Phys. B: At. Mol. Opt. Phys., 43, (2010) 163001.
[16] Y.M. Andreeva, M.M. Sergeev, R.A. Zakoldaev, U.E. Gabysheva, V.P. Veiko, E.B. Yakovlev, S.I. Kudryashov, P.A. Danilov, A.A. Ionin, F. Vocanson, T.E. Itina, T.V. Antropova, O.S. Medvedev: J. Laser Micro Nanoeng., 13, (2018) 193.
[17] A.Couairon, A.Mysyrowicz: Phys. Rep, 441, (2007) 47.

ISSN:1300-669
Volume 16 Issue 2 July 2020

[18] Yongfeng Ju, Yang Liao, Long Zhang, Yinglong Sheng, Qiang Zhang, Danping Chen, Ya Cheng, Zhizhan Xu, Koji Sugioka, and Katsumi Midorikawa: Microfluid Nanofluid, 11, (2011) 111.
[19] Yang Liao, Yongfeng Ju, Long Zhang, Fei He, Qiang Zhang, Yinglong Shen, Danping Chen, Ya Cheng, Zhizhan Xu, Koji Sugioka, and Katsumi Midorikawa: Opt. Lett., 35, (2010) 3225.
[20] S Nikumb, Q Chen, C Li, H Reshef, HY Zheng, H Qiu, D Low: Thin Solid Films, 477, (2005) 216.

(Received: July 8, 2021, Accepted: November 13, 2021)